Analytical Methods

ROYAL SOCIETY OF CHEMISTRY

PAPER

Cite this: *Anal. Methods*, 2020, **12**, 959

Assessment of ATR-FTIR spectroscopy with multivariate analysis to investigate the binding mechanisms of Ag and TiO_2 nanoparticles to Chelex®-100 or Metsorb™ for the DGT technique†

Hamid Pouran, *[a] Rosario Perez Colodrero, [a] Shuang Wu,[b] Gary Hix,[a] Julia Zakharova[a] and Hao Zhang[b]

Studying nanomaterials' ecotoxicology is not new but there are still gaps in our understanding of their fate in the environment. A major challenge is lack of reliable tools to measure available concentrations of nanoparticles (NPs) in soil and water. Diffusive gradients in thin-films (DGT) is a robust technique for measuring the concentrations of trace metals in the environment. We have also shown that it could be potentially developed for measuring ZnO NPs. To further investigate the suitability of DGT for measuring the available concentrations of NPs in soil and water we selected two model nanoparticles, Ag and TiO_2, which are widely used and incorporated in different commercial products. We aimed to understand (1) if two of the DGT binding agents, Chelex®-100 and Metsorb™, could irreversibly retain our model NPs and if yes (2) what might be the differences between bound Ag and TiO_2 NPs and Ag^+ and Ti^{4+} cations. We used ATR-FTIR spectroscopy for this purpose and analysed the IR spectra using principal component analysis and linear discriminant analysis (PCA-LDA), as our pattern recognition tool. The results show that the DGT resins form chemical bonds with silver and titanium nanoparticles and their ionic forms. PCA-LDA demonstrates that the binding mechanisms are statistically different (95% confidence level) among the treatments. This study indicates DGT's potential for measuring the available concentrations of NPs in the environment and suggests that ATR-FTIR spectroscopy combined with computational analysis could potentially differentiate between chemical species that are retained simultaneously by the DGT device resin layer.

Received 14th November 2019
Accepted 9th January 2020

DOI: 10.1039/c9ay02458a

rsc.li/methods

1. Introduction

Diffusive gradients in thin-films which is often known as the DGT technique is a simple, yet accurate and reliable approach for measuring time-averaged concentrations of different chemicals in soil and water.[3–6] A DGT device is comprised of two key components; a diffusive hydrogel layer and a binding layer, which are protected by an external filter membrane and placed on a plastic base. A plastic cap keeps the filter membrane, the diffusive (hydrogel) and binding layers in place on top of the plastic base (piston) as illustrated in Fig. 1. The function of each part of the DGT device and their detailed features have been described extensively in previous studies.[7,8]

The DGT technique is based on the concept that the target chemical species passing through the diffusive layer are irreversibly retained by the binding resin. With the known thicknesses of the diffusion layer, diffusion coefficients of the retained species, the surface area of the exposure window, the length of time and ambient temperature during the DGT deployment, the time averaged concentration of the retained chemicals can be determined using the DGT equation, which is based on Fick's law of diffusion.[8]

A crucial step for measuring the time-averaged concentration of a chemical by DGT is its ability to pass through the diffusive layer and be retained by the binding layer. In our previous research we showed that the DGT technique can potentially measure the concentrations of manufactured nanomaterials in the environment,[2] an approach which was

[a]*Faculty of Science and Engineering, University of Wolverhampton, WV1 1LY, UK. E-mail: hamidpouran@gmail.com; Tel: +44 (0)7930342062*

[b]*Lancaster Environment Centre, Lancaster University, Bailrigg, Lancaster, LA1 4YQ, UK*

† Electronic supplementary information (ESI) available: Surface potential of Ag and TiO_2 NPs used in this experiment. Derived infrared (IR) spectra of Metsorb exposed to the titanium dioxide nanoparticle treatments. Three-dimensional score plot visualization of principal component analysis and linear discriminant analysis (PCA-LDA) of Metsorb exposed to TiO_2 treatments. Two-D visualization of principal component analysis and linear discriminant analysis (PCA-LDA) of Chelex®-100 and Metsorb™ when exposed to silver samples; (1) Ag NPs, (2) Ag^+, and (3) a mixture of Ag NPs and the titanium treatments; (4) TiO_2 NPs, (5) Ti^{4+}, and (6) a mixture of TiO_2 NPs and Ti^{4+}. Scanning electron microscopy (SEM) images of Chelex®-100 and Metsorb™ exposed to Ag and TiO_2 NPs. See DOI: 10.1039/c9ay02458a

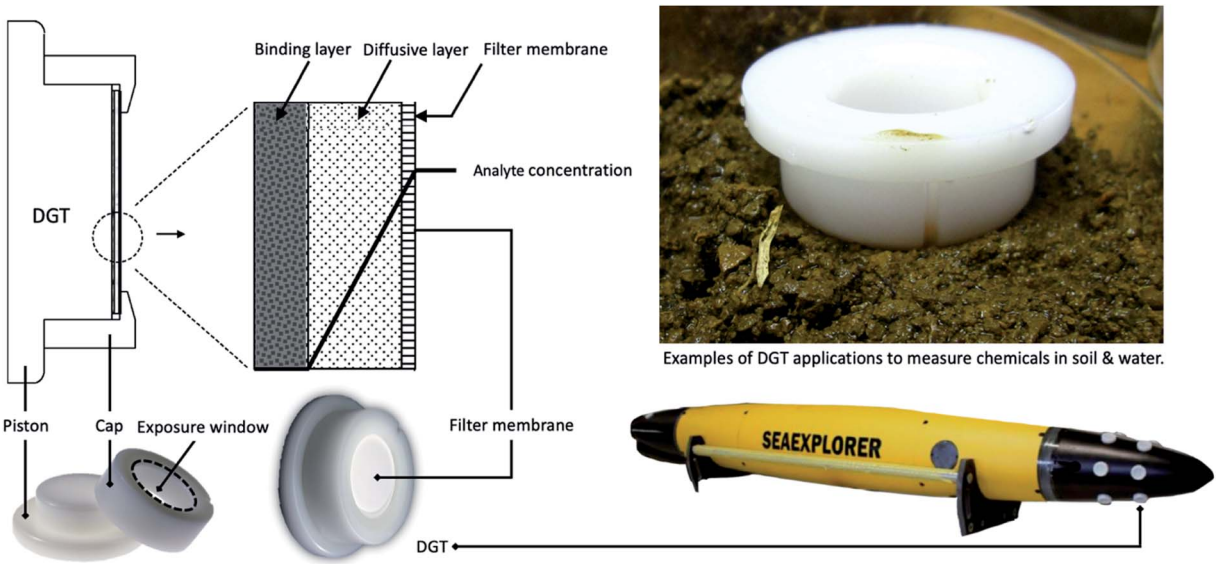

Fig. 1 Schematic representation of a DGT device and its components in addition to its application in soil and water as illustrated in other research.[6]

promisingly repeated in other research using the same principles.[9–13] We used combinations of different membranes and diffusive gels to allow certain sizes of particulate matter to enter the device for measuring different targeted chemical species.[3] The most commonly used diffusive gels in the DGT technique are agarose, open pore polyacrylamide and restricted polyacrylamide gels. Each of them has different pore sizes. Some studies suggest that particles as large as 100 nm can diffuse through open pore hydrogels.[14] For the binding layers, Chelex®-100, Metsorb™ and Fe-oxide gels are often used in the DGT devices.[1,2,8,15]

We have previously studied the binding mechanism of ZnO nanoparticles (NPs) and Zn^{2+} to Chelex®-100 and Metsorb™ as two commercially available and widely used binding resins.[1,2,5] In this study, we focus on using the same resins for two industrially important and extensively made nanomaterials;[16,17] Ag and TiO_2 nanoparticles and their ionic forms Ag^+ and Ti^{4+}. Chelex®-100 is an ion-exchange resin with efficient binding surfaces, which stems from its chemical structure. It includes dicarboxylic acid amine ($COOHCH_2$–NH–$COOHCH_2$) with carboxyl groups, which deprotonate at relatively low pH values (pH $\approx$ 4).[18]

Less information is available about the Metsorb™ chemical structure compared to Chelex®. This commercial material is mainly a titanium oxide-based resin with TiO_2 and $Ti(OH)_4$ as its main constituents and small quantities of other chemicals including polymers.[19] Both titanium oxide/hydroxide constituents in Metsorb™ have a low point of zero charge (PZC, the pH at which the overall surface charge is neutral), which makes its surface to pose overall negative surface charge at the pH of natural environments. These pH values (PZC) are approximately 4.5 for $Ti(OH)_4$ and 6.0 for TiO_2.[5,20,21]

Both Chelex®-100 and Metsorb™ have been used extensively as binding materials in DGT devices for measuring targeted chemical species in soil and water.[6] We have also shown that these two resins are capable of retaining ZnO nanoparticles and potentially could be deployed for measuring nanomaterials in the environment.[8,22] The performance of Chelex®-100 and Metsorb™ and their reliable function as binding materials in the DGT devices for ionic metals and nutrients have been studied before, nevertheless limited information is available about their potential for nanomaterials.[23,24] Studying the binding mechanisms of chemicals to the aforementioned resins helps us to better investigate their suitability for using in the DGT technique to measure time averaged concentrations of the nanomaterials in the environment.

The aim of this research is to investigate how Chelex®-100 and Metsorb™ retain four different chemicals, Ag and TiO_2 nanoparticles and their ionic forms Ag^+ and Ti^{4+}. For this purpose, we used attenuated total reflection-Fourier transform infrared (ATR-FTIR) spectroscopy, followed by principal component analysis (PCA) and linear discriminating analysis (LDA) to further process the ATR-FTIR data. ATR-FTIR spectroscopy is widely used for exploring chemical interactions at solid–liquid interfaces for both organic and inorganic samples and as a non-destructive technique.[25–27] It will provide information to elucidate the underlying differences between these nanoparticles and their ionic forms chemically bonded to the DGT resins. Ag and Ti nano-particles are widely used in different industries as engineered nanomaterials. Previous studies indicate that after waste treatment processes, they likely re-enter the environment and accumulate in soils as their primary sink. This may lead to bioaccumulation in microorganisms and plants and affect the food chain.[5,28] Measuring these nanomaterials' concentrations in soil and water helps us to better understand their behavior in the environment.

Silver nanoparticles are well known for their antimicrobial properties and used in many industries particularly in personal

care products and clothing *e.g.* in textiles to eliminate bacteria and odor. These nanoparticles also have unique physicochemical characteristics (*e.g.* electrical and thermal conductivity), which make them attractive for many industries, for example food packaging, cosmetics and biomedical related products, increasing their risk of being released to the environment.[29,30] Titanium dioxide nanoparticles are stable in the environment with desirable photocatalytic properties, they have a high refractive index, which makes them excellent white powder pigments, with extensive applications as coating or paint materials. Both of these nanomaterials are shown to have adverse environmental impacts when they are released to the environment, especially in high concentrations, which makes probing their concentrations in the environment essential.[17]

2. Experimental section

2.1. Materials and methods

2.1.1 Chemicals. TiO_2 was obtained from EVONIK (AEROXIDE® TiO_2),[31] and Ag nanoparticles were sourced from Institut Català de Nanotecnologia, Spain. The silver nanoparticles were polyvinylpyrrolidone (PVP 9.73%) with primary particle sizes expected to be approximately 25 nm. Detailed properties of these Ag nanoparticles, provided by the above-mentioned supplier, have been described in other studies.[16] The primary particle size of the TiO_2 NPs was expected to be approximately 50 nm. Point of zero charge (PZC) of Ag is usually below pH ≈ 4, while it is about pH ≈ 6 for TiO_2 NPs,[17,32] which create, respectively, negative and positive zeta potential (electrokinetic potential) at the surface of these nanoparticles in this study. Some details can be found in the ESI.† The DGT resin materials, Chelex®-100 and Metsorb™, were purchased from Bio-Rad and Graver Technologies. Before each test, fresh stock solutions of Ag and TiO_2 nanoparticle dispersions in Milli-Q water were prepared, followed by sonication for at least 15 minutes. Fresh stock solutions of Ag^+ were prepared by dissolving Sigma-Aldrich reagent grade $Ag(NO_3)$ in Milli-Q water. For the Ti^{4+} stock solution, acidified Sigma-Aldrich reagent grade $TiCl_4$ was used.

2.1.2 Sample preparation. Each experimental treatment sample for ATR-FTIR spectrochemical analysis was prepared in triplicate. For this purpose, 0.5 g of Chelex®-100 or Metsorb™ (binding materials) was exposed to 20.0 ml of 1000.0 μg l^{-1} of one of six different treatments; (1) Ag NPs, (2) Ag^+, (3) a mixture of Ag NPs and Ag^+ (500 μg l^{-1} each), (4) TiO_2 NPs, (5) Ti^{4+}, and (6) a mixture of TiO_2 NPs and Ti^{4+} (500 μg l^{-1} each), which correspond to six different spectral classes for each of the resins. We used high concentrations for each of these treatments to enable reliable detection by ATR-FTIR spectroscopy. The pH for all the experiments in this study was approximately 5.8. For the Ti^{4+} stock solution, which had been prepared from acidified $TiCl_4$, the pH was adjusted by adding a very dilute NaOH solution (reagent grade). The pH values were monitored for 48 hours throughout the experiments.

Each sample of a fresh chemical solution with the resin was shaken for over 3 hours on a rotary shaker at 150 rpm. Then they were centrifuged for 20 minutes at 3500 rpm and the supernatant was discarded. The resins were washed by adding 50 ml of Milli-Q water, shaking for further 30 minutes and centrifugation as before. This process was repeated three times to remove residuals that may be attached physically on the resins but not retained by chemical binding. The samples were dried by pressurized nitrogen gas (0.4 bar) and a small portion of each dry sample was put on the ATR crystal for ATR-FTIR spectroscopy analysis as illustrated in Fig. 2. The samples prepared for the analysis completely covered the ATR crystal and provided a thickness of over 3 μm to eliminate any interference that could be caused by the compression rod that keeps the samples in place.

2.1.3 Spectral acquisition and data processing. A PerkinElmer Spectrum 100 FTIR Spectrometer was used for data acquisitions (Fig. 2). Each experiment was conducted in

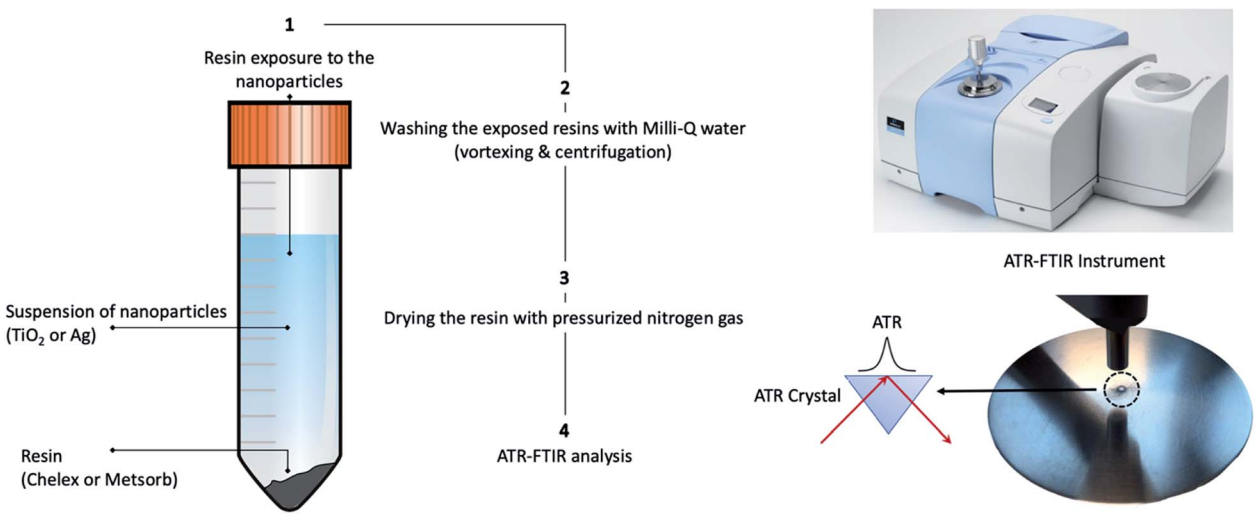

Fig. 2 Schematic representation of the experimental procedure. Exposing Chelex®-100 and Metsorb™ to Ag and TiO_2 NP suspensions and their ionic forms for spectral acquisition.

triplicate and for each sample, 30 spectra were acquired at a 2 cm^{-1} spectral resolution. The IR spectra covering the 600–4000 cm^{-1} range were divided into three different spectral regions: region one 600–800 cm^{-1}; region two, 800–2200 cm^{-1}; and, region three, 2600–4000 cm^{-1}. To compare the spectral classes, baseline corrections (rubber band) and vector normalization were used for all of the regions for each treatment. Details of these techniques and available tools to perform these analyses have been described in previous studies.[33–35]

Following this step, the spectral data were further processed using principal component analysis (PCA) coupled with linear discriminating analysis (LDA), which is often referred to as PCA-LDA. Both PCA and LDA are statistical procedures and data transformation techniques used in a range of engineering concepts to classify different data and identify patterns. PCA can be described as a linear dimensionality reduction method to project the data into the directions of highest variability (where the data are most spread), while LDA computes the

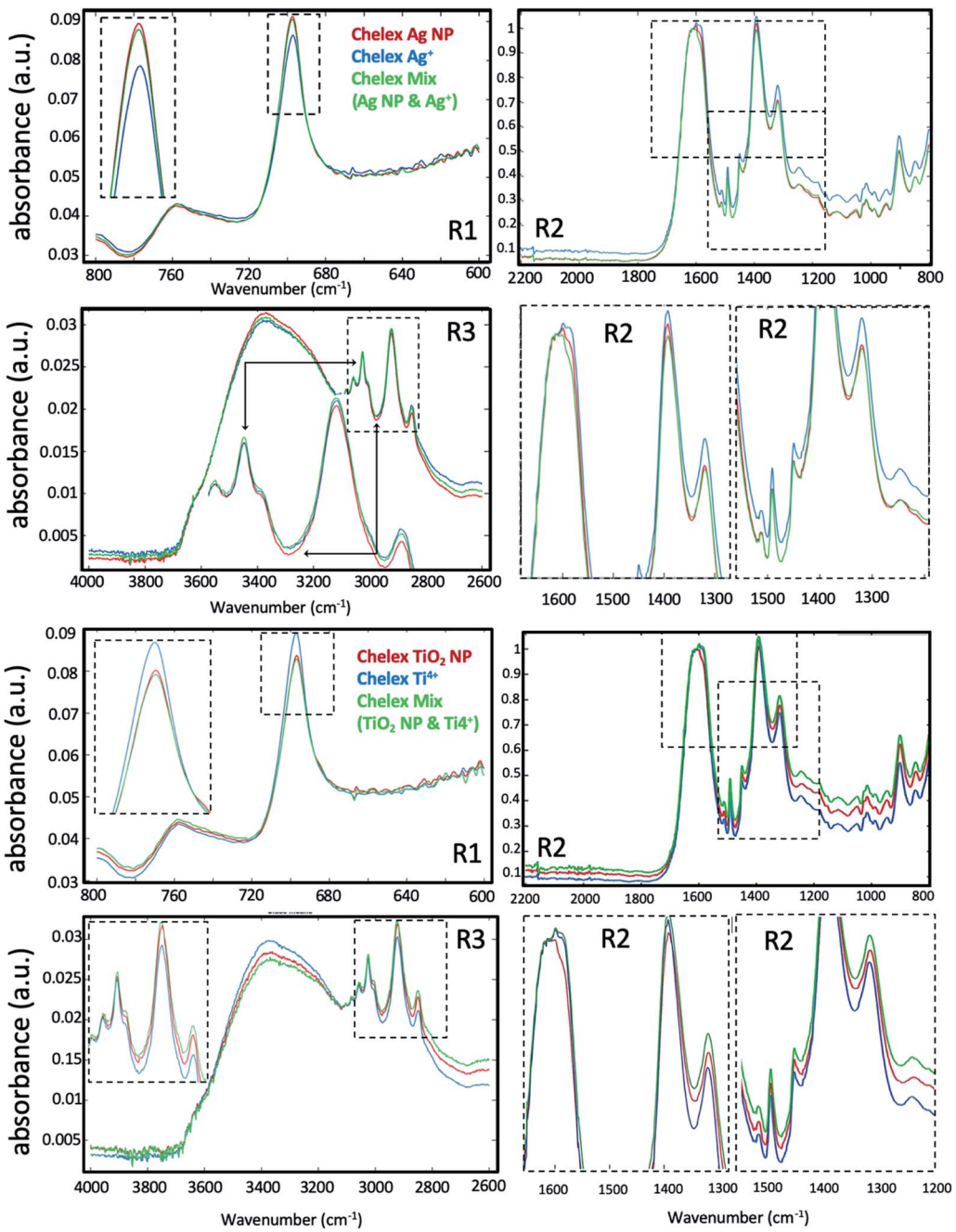

Fig. 3 Comparison between the derived infrared (IR) spectra of Chelex-100 exposed to the silver and titanium dioxide treatments. The IR spectra (600–4000 cm^{-1}) are divided into three spectral regions: region 1 (600–800 cm^{-1}), region 2 (800–2200 cm^{-1}), and region 3 (2600–4000 cm^{-1}) for comparison purpose.

highest possible discrimination between different classes of data which helps us to classify the data accurately.[36,37]

In this study we used PCA to reduce the number of variables in the spectral data (*i.e.*, absorbance intensities at different wavenumbers) to only a few factors that can capture >95% variance of the dataset. If the within-class variation is larger than what is found between classes, LDA can be applied to the output from PCA to minimize the within-class variation and maximize the between-class variation. This allows us to identify the most important discriminating information and remove interference from the data as described in previous research.[1,2,33] In other words, this method helps us to identify class differences through the generation of scores and plots. As seen in the following sections, in an LDA score plot each spectrum represents a point in LDA space and classes tend to form clusters. In these clusters the closeness between points implies spectral similarities while the distance signifies class dissimilarities. Also, the plots can be used to identify chemical bonds distinguishing different treatment conditions.

In addition to IR spectroscopy and pattern recognition analysis, we investigated binding of Ag and TiO_2 NPs on Chelex®-100 and Metsorb™ using a scanning electron microscope (SEM) to provide further evidence for retention of these NPs on the resins (see the ESI† for details).

3. Results and discussion

Fig. 3 and 4 show different regions of the IR spectra obtained from Chelex®-100 and Metsorb™ after their exposure to silver and titanium dioxide nanoparticles and their ionic forms. As described earlier there are six different spectral classes for each resin, of which three of them belong to silver samples; (1) Ag NPs, (2) Ag^+, and (3) a mixture of Ag NPs and Ag^+, and the other three belong to the titanium treatments; (4) TiO_2 NPs, (5) Ti^{4+}, and (6) a mixture of TiO_2 NPs and Ti^{4+}. As seen in these figures clear alterations are observed in different peak absorbance intensities or slight shifts in wavenumbers.

Both of the resins in this study are known for their abilities to bind cations because of their surface functional groups.[1,8,38] Fig. 5 is a schematic representation of potential chemical bonds that may form between the binding agents and Ag^+ and Ti^{4+} cations. Chelex®-100 carboxyl and Metsorb™ surface titanium oxide/hydroxide hydroxyl groups can bind available Ag^+ and Ti^{4+} and irreversibly retain them. Deprotonation of carboxyl groups in Chelex®-100 occurs normally at pH $\approx$ 4.0, thus its overall surface charge in all the experiments with pH $\approx$ 5.8 is negative.[2,18] Details of the Metsorb™ chemical structure are not fully disclosed, nevertheless we know that titanium oxides, TiO_2 and $Ti(OH)_4$, are the main components of this commercial product with TiO_2 being dominant. The point of zero charge of Metsorb™ is pH $\approx$ 6.0 (ref. 19 and 39) and it has overall neutral to slightly positive surface charge under the current experimental conditions (pH $\approx$ 5.8) (see the ESI† for details).

It is worth noting that at any given pH, both protonated and deprotonated functional groups exist at the same time on the resin surface, but their ratio is affected by the concentration of protons.[26,40] Deprotonated surface functional groups on Chelex®-100, carboxyl groups as seen in Fig. 5, could bind Ag^+ or Ti^{4+} directly. Also, two adjacent carboxyl groups are able to chemisorb these cations, while hydroxyl and carbonyl groups

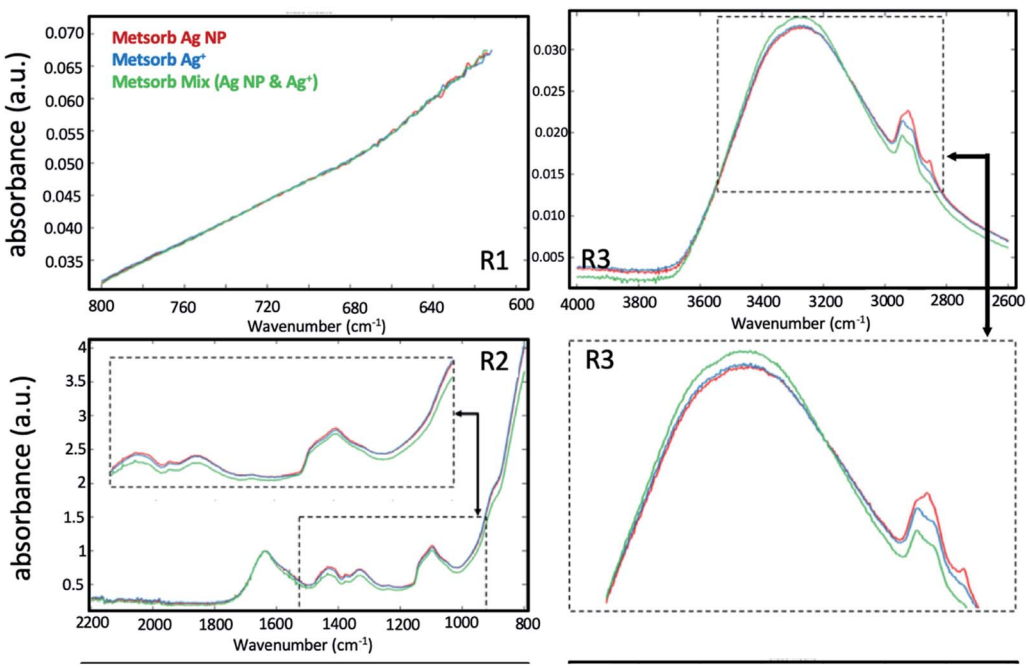

Fig. 4 Comparison between the derived infrared (IR) spectra of Metsorb exposed to the silver nanoparticle and Ag^+ treatments. The IR spectra (600–4000 cm^{-1}) are divided into three spectral regions: region 1 (600–800 cm^{-1}), region 2 (800–2200 cm^{-1}), and region 3 (2600–4000 cm^{-1}) for comparison purposes (see the ESI† for the IR spectroscopy results of Metsorb exposed to titanium dioxide nanoparticles).

together could form complexes with them. Ag NP carries overall negative surface charge in this experiment. Its surface includes oxidized, protonated and deprotonated sites that co-exist at the same time on an Ag NP surface. Chemical bonds could form between protonated surface hydroxyl groups of Ag NPs and deprotonated carboxyl. Other bindings between structural Ag at the surface of Ag NPs and carboxyl carbonyl and hydroxyl groups are also possible. The same occurs when Chelex®-100 is exposed to TiO_2 NPs, however, we know that the majority of hydroxyl groups formed on the surface of titanium dioxide nanoparticles are protonated in this study, which could lead to stronger bond formation and retention of this nanoparticle by Chelex®-100.

As illustrated in Fig. 5, surface deprotonated hydroxyl groups of Metsorb™ could form chemical bonds with Ag^+. To a lesser extent compatible bindings could occur between Metsorb™ constituent chemicals and its surface functional groups with Ag NPs (structural silver and protonated and deprotonated surface hydroxyl groups that form on this nanoparticle surface).[1,26,27,40]

The aforementioned bonding characteristics should be reflected in the vibrational changes of the IR spectra of the samples.[27,41] Fig. 3 and 4 represent the IR spectra of these chemicals in more detail. In spectral region one (600–800 cm^{-1}), Chelex®-100 treatments result in a notable alteration at $\approx$700 cm^{-1} with clear distinction (peak intensities and a slight shift in wavenumbers) between the different classes of the spectra, but changes for the peak at $\approx$760 cm^{-1} seem to be negligible. Interestingly, for Chelex®-100 silver and titanium treatments show different patterns. At $\approx$700 cm^{-1} Ag NPs and the mixture of Ag NPs and Ag^+ have a stronger peak (more absorbance) compared to Ag^+. For the titanium samples, we have an opposite behavior and Chelex®-100 exposed to Ti^{4+} has

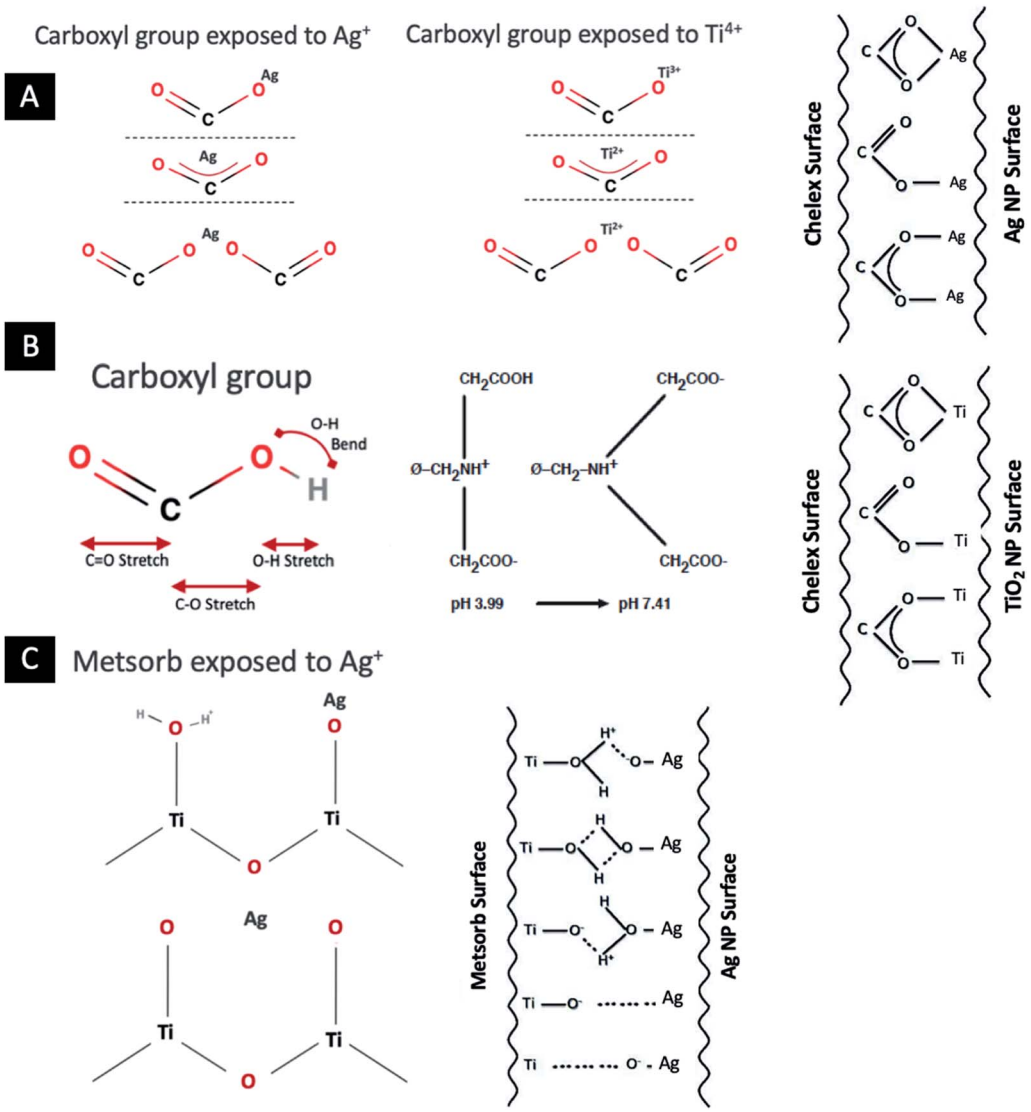

Fig. 5 Schematic representation of some of the major chemical bonds that could form between the Chelex-100 carboxyl group with Ag^+ and Ti^{4+} (A). Chemical structure of Chelex-100, its deprotonation and carboxyl group potential vibrations (B). Some of the major chemical bonds that could form between Metsorb and Ag^+ (C). Also, potential bond formation between the surfaces of Ag, TiO_2 NPs and Chelex-100 or Metsorb has been illustrated on the left side of this figure.

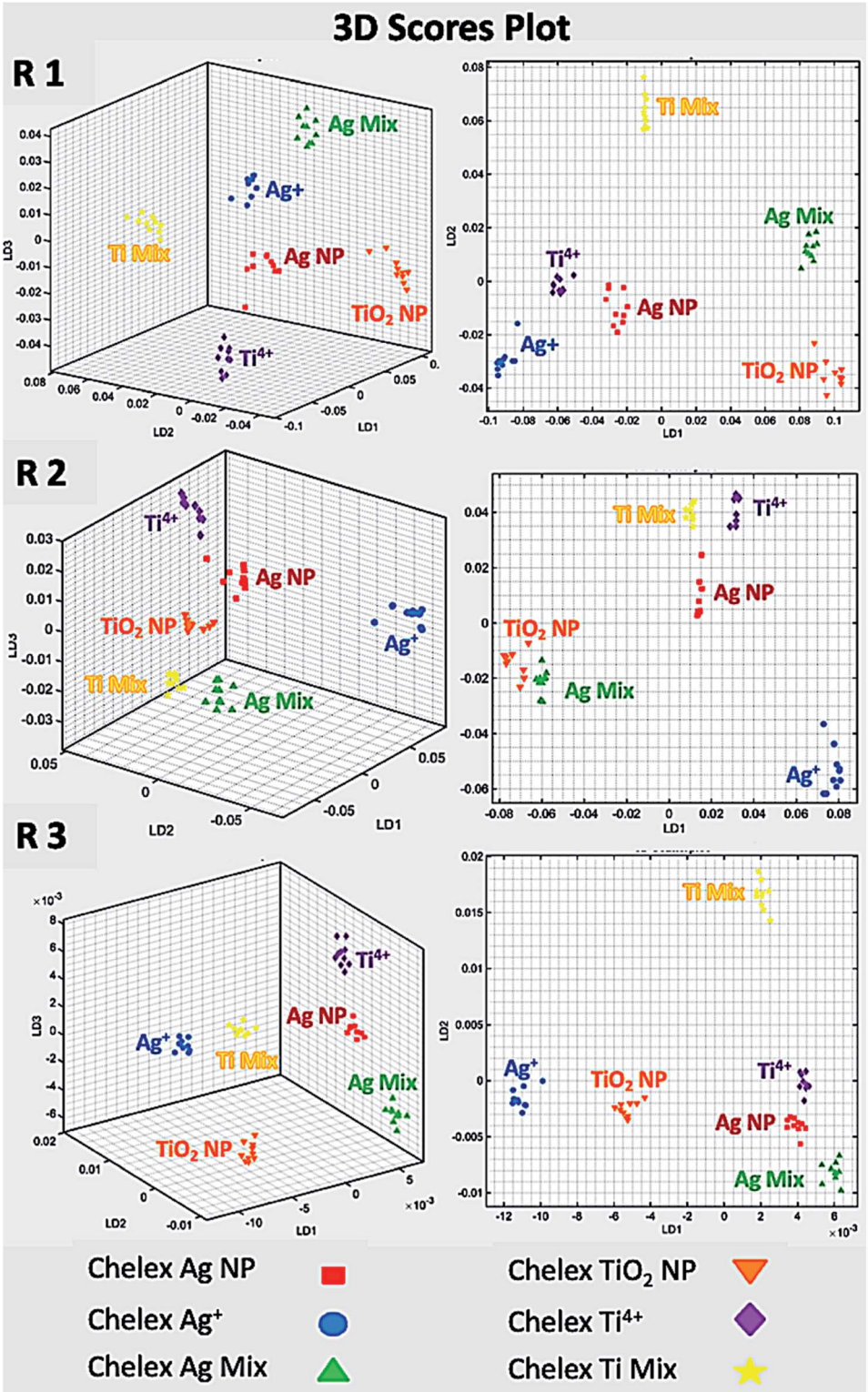

Fig. 6 Three-dimensional score plot visualization of principal component analysis and linear discriminant analysis (PCA-LDA) of Chelex-100 when exposed to Ag and TiO_2 treatments. R1 (600–800 cm^{-1}), R2 (800–2200 cm^{-1}), and R3 (2600–4000 cm^{-1}), respectively, represent three spectral regions of the spectra. Scales for *X*, *Y*, and *Z*-axes are arbitrary units. The graphs on the right show the top views of these score plots.

a stronger peak compared to TiO_2 NPs or the mixture of Ti^{4+} and TiO_2 NPs. The peak at ≈760 cm^{-1} is broader, has considerably less strength compared to the one at ≈700 cm^{-1} and the observed changes are minor (because of the similarities of the peak intensities). These peaks can be assigned to C–H and N–H vibrations, respectively.[25,42]

The differences between these peaks at ≈700 cm^{-1} could stem from stronger polarity of chemical retention that occurs between C–H and Ag NPs. A higher number of the same chemical bonds between the resin and Ag NPs could also contribute to a higher peak intensity. In contrast, it seems that for Chelex®-100 titanium treatments, it is Ti^{4+} that creates a stronger dipole moment and therefore a stronger peak. For Metsorb™, the skewed broad peak that is extended to ≈800 cm^{-1} can be attributed to metal oxygen bond vibrations that are present in the titanium oxide in Metsorb™.[2,43]

In region two of the spectra, Chelex®-100 treatments show alterations at ≈900 cm^{-1} (C–H out-of-plane bending), ≈1330 cm^{-1} (O–C stretching), ≈1400 cm^{-1} (C–O–H in plane bending), ≈1430 cm^{-1} (O=C–O stretching of carboxylate group), ≈1500 cm^{-1} (N–H bending), and ≈1620 cm^{-1} (C=O stretching).[25,26,42] These changes suggest variations in the strength of chemical bonds between oxygen (from C–O, O=C–O and C=O) and Ag^{+} or Ti^{4+}, structural Ag of Ag NPs or Ti of TiO_2 NPs, or the surface hydroxyl groups formed on these nanoparticles. As described earlier Metsorb™ is mainly made

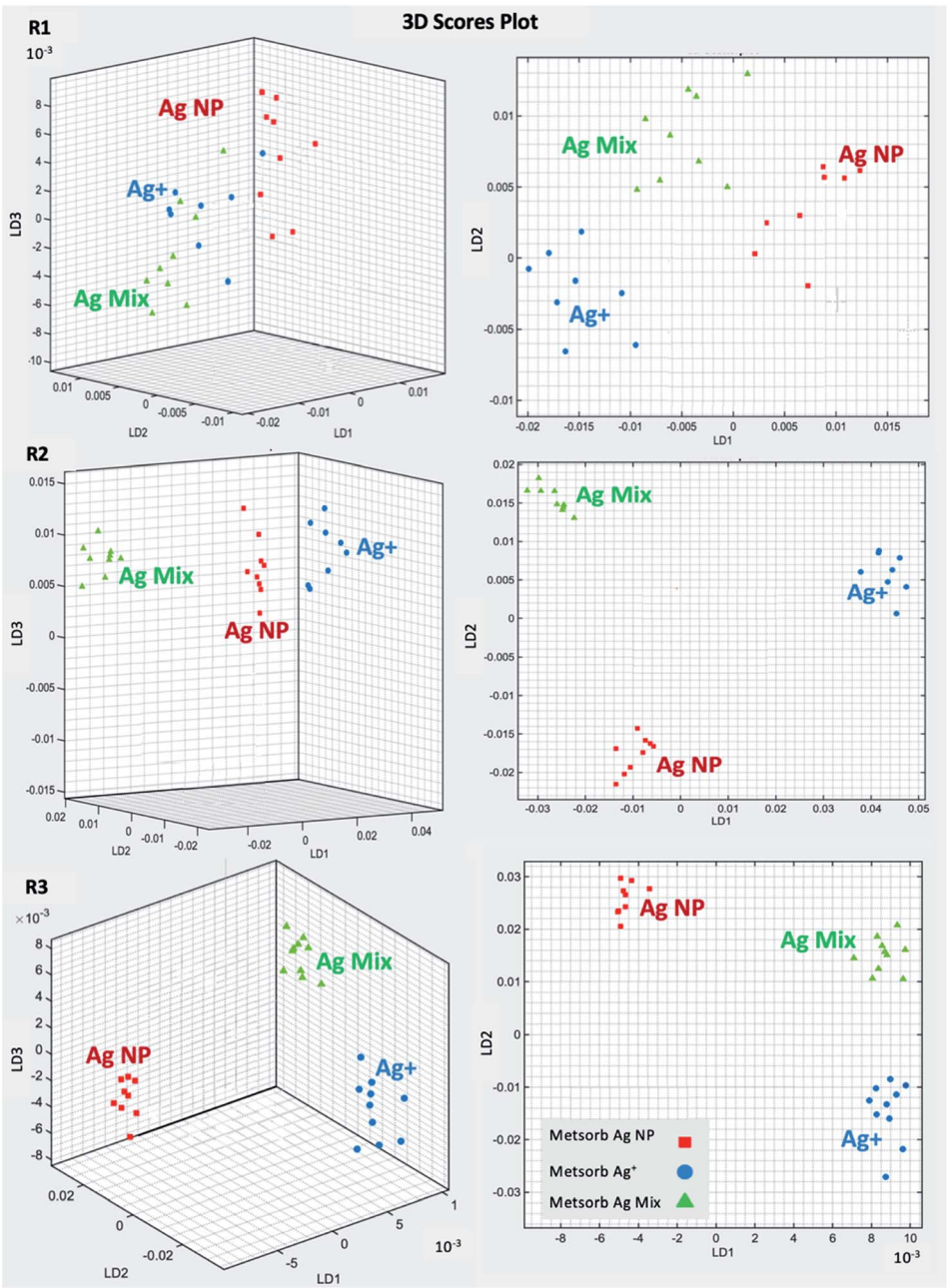

Fig. 7 Three-dimensional score plot visualization of principal component analysis and linear discriminant analysis (PCA-LDA) of Metsorb when exposed to Ag treatments. R1 (600–800 cm^{-1}), R2 (800–2200 cm^{-1}), and R3 (2600–4000 cm^{-1}), respectively, represent three spectral regions of the spectra. Scales for *X*, *Y*, and *Z*-axes are arbitrary units. The graphs on the right show the top views of these score plots (see the ESI† for PCA-LDA score plot visualization of Metsorb exposed to titanium dioxide nanoparticles).

of titanium oxide, however, it has some impurities including ethanol (C_2H_4O).[2,19] Bands in the second region of this resin's spectra at ≈1100 cm^{-1}, ≈1350 cm^{-1} and ≈1440 cm^{-1} are likely because of the C–OH stretch, C–OH and O–H in-plane bend, respectively.[25,42,43] From these peaks it could be inferred that the surface hydroxyl groups are involved in bond formation with Ag^+ and/or Ag NPs. The peak at ≈1650 cm^{-1} can be attributed to the bending mode of H–O–H, resulting from vibration of water or protonation of surface hydroxyl groups.[44]

For Chelex®-100 we see a broad O–H stretch peak in region three, which spans from ≈2800 cm^{-1} to ≈3600 cm^{-1}; N–H stretching vibrations at ≈3400 cm^{-1} could also contribute to this peak. Symmetric and asymmetric stretching of C–H and =C–H stretching could be the reason for multiple bands seen at ≈2850 cm^{-1}, ≈2920 cm^{-1} and ≈3030 cm^{-1}.[27] For the Metsorb™ spectra in region three O–H stretching can be identified as a broad peak at ≈3100–3600 cm^{-1} and the other peak, which appears at ≈2950 cm^{-1}, can be assigned to Ti–OH bending.[43] Changes in intensities and shifts in these wavenumbers could be the result of the variations in electrostatic attractions between Ag^+ and structural Ag and surface hydroxyl groups of Ag NPs with functional groups of these vibrational bands.[1,2] As mentioned earlier, in addition to stronger dipole moments between the bound entities, an increase in peak intensity could be attributed to an increase in the number of functional groups and surface sites associated with the chemical bonds that lead to the observed differences among the samples.

Fig. 6 and 7 are 3-D score plots that exhibit PCA-LDA of the absorbance spectra of Chelex®-100 and Metsorb™. Details of this computational analysis method are available in previous publications.[2,33–35] As seen multivariate analysis suggests that silver treatments and titanium samples form distinguishable and separate clusters of data in both Chelex®-100 and Metsorb™, which indicate that components of each of these groups have clear differences from each other. In these figures the 3-D scatter plots separate the analyzed (PCA-LDA) IR spectra based on their characteristic differences in their absorbance.[1,2,33] These analyses demonstrate that for the derived spectra of Chelex®-100, all of the treatments, (1) Ag NPs, (2) Ag^+, (3) a mixture of Ag NPs and Ag^+, (4) TiO_2 NPs, (5) Ti^{4+}, and (6) a mixture of TiO_2 NPs and Ti^{4+}, are statistically different at the 95% confidence level (for more details, see the ESI†). In other words, these six different spectral classes show statistically different absorbance. For Metsorb™, as Fig. 7 demonstrates, silver samples form three different clusters, which are separated from each other. This segregation indicates that the Metsorb™ spectra of these treatments have different characteristics.

In this study the binding mechanisms of the two nanoparticles and their ionic forms to Chelex®-100 and Metsorb™ are affected by the strength and number of chemical bonds formed between them. For Ag^+ and Ti^{4+} the resins attract readily available cations, which have a similar size to the binding sites on these resins, but for Ag and TiO_2 NPs they interact with structural Ag and Ti or functional groups formed on their surfaces including hydroxyls. In addition, Ag NPs carry overall negative surface charge at the pH of the experiment while TiO_2 NPs have overall positive surface pH dependent charge in this experiment (see ESI†). Such surface charges influence electrostatic interactions that occur between Chelex®-100 with negative surface charge and Metsorb™ with neutral to slightly positive surface charge at the pH of the experiment (pH ≈ 5.8). When Chelex®-100 or Metsorb™ is exposed to Ag or TiO_2 NPs chemisorption occurs between two surfaces, with impacts on the polarity of chemical bonds formed between the two entities and the number of functional groups involved in sorption of the NPs, both of which influence intensities of the absorbance peaks in the IR spectra. This is compatible with what we observed in the IR spectra of the treatments and deducted through computational analysis and pattern recognition using the PCA-LDA technique. It's worth highlighting that this research provides a key finding with respect to the diffusive gradients in thin-film (DGT) technique and confirms that Chelex®-100 or Metsorb™ resins, which are of the most common binding materials in DGT devices, are able to form chemical bonds with two of the most extensively used nanomaterials in the world. Considering the well-established DGT technique for measuring time-averaged concentrations of chemicals in the environment, the findings here could pave the road for further development of DGT for measuring Ag and Ti nanoparticles in the environment and helping us to improve our understanding of the fate and the behavior of these materials in nature. In addition to ATR-FTIR spectroscopy and PCA-LDA analysis, we have also used scanning electron microscopy (SEM) imaging. The SEM images showed the presence of Ag and TiO_2 nanoparticles on the Chelex®-100, however because of the physical appearance and porous structure of Metsorb™ we couldn't identify these nanoparticles on the surface of this resin. The results can be seen in the ESI.†

4. Conclusions

This research shows that Ag and TiO_2 nanoparticles form chemical bonds with Chelex®-100 and Metsorb™, which are two commonly used binding resins in the diffusive gradients in thin-film (DGT) method. It reinforces our previous findings about DGT potential for measuring engineered nanomaterials in soil and water[1,2] and is compatible with other studies.[9–13] This study also suggests that ATR-FTIR spectroscopy in combination with principal component analysis (PCA) and linear discriminating analysis (LDA), or other pattern recognition methods, could be developed to identify different types of chemicals retained by the binding resins. These give the confidence for using the DGT technique for measuring nanoparticles in the environment. However, further tests that include investigating diffusional characteristics of models Ag and TiO_2 in the DGT diffusive layers and the performance under a range of environmental conditions are required. Further development of the DGT technique for measuring engineered nanomaterials *in situ* in soils and waters would allow us to have a better understanding of their behavior in the environment.

Conflicts of interest

There are no conflicts to declare.

References

1 H. M. Pouran, V. Llabjani, F. L. Martin and H. Zhang, Evaluation of ATR-FTIR Spectroscopy with Multivariate Analysis to Study the Binding Mechanisms of ZnO Nanoparticles or Zn to Chelex-100 or Metsorb, *Environ. Sci. Technol.*, 2013, **47**(19), 11115–11121.

2 H. M. Pouran, F. L. Martin and H. Zhang, Measurement of ZnO nanoparticles using diffusive gradients in thin films: binding and diffusional characteristics, *Anal. Chem.*, 2014, **86**(12), 5906–5913.

3 *Diffusive Gradients in Thin-Films for Environmental Measurements*, ed. W. Davison and H. Zhang, Cambridge University Press, Cambridge, 2016.

4 H. Zhang and W. Davison, In situ speciation measurements. Using diffusive gradients in thin films (DGT) to determine inorganically and organically complexed metals, *Pure Appl. Chem.*, 2001, **73**(1), 9–15.

5 H. M. Pouran, Engineered Nanomaterials in the Environment, their Potential Fate and Behaviour and Emerging Techniques to Measure Them, in *Handbook of Environmental Materials Management*, Springer International Publishing, Cham, 2018, pp. 1–15.

6 W. Baeyens, Y. Gao, W. Davison, J. Galceran, M. Leermakers, J. Puy, P.-J. Superville and L. Beguery, In situ measurements of micronutrient dynamics in open seawater show that complex dissociation rates may limit diatom growth, *Sci. Rep.*, 2018, **8**(1), 16125.

7 H. Zhang, W. Davison, B. Knight and S. McGrath, In situ measurements of solution concentrations and fluxes of trace metals in soils using DGT, *Environ. Sci. Technol.*, 1998, **32**, 704–710.

8 W. Davison and H. Zhang, Progress in understanding the use of diffusive gradients in thin films (DGT) – back to basics, *Environ. Chem.*, 2012, **9**(1), 1–13.

9 N. Odzak, D. Kistler, R. Behra and L. Sigg, Dissolution of metal and metal oxide nanoparticles in aqueous media, *Environ. Pollut.*, 2014, **191**, 132–138.

10 A. L.-T. Pham, C. Johnson, D. Manley and H. Hsu-Kim, Influence of Sulfide Nanoparticles on Dissolved Mercury and Zinc Quantification by Diffusive Gradient in Thin-Film Passive Samplers, *Environ. Sci. Technol.*, 2015, **49**(21), 12897–12903.

11 R. Sekine, G. Brunetti, E. Donner, M. Khaksar, K. Vasilev, Å. K. Jämting, K. G. Scheckel, P. Kappen, H. Zhang and E. Lombi, Speciation and Lability of Ag-, AgCl-, and Ag_2S-Nanoparticles in Soil Determined by X-ray Absorption Spectroscopy and Diffusive Gradients in Thin Films, *Environ. Sci. Technol.*, 2015, **49**(2), 897–905.

12 S. Liu, N. Qin, J. Song, Y. Zhang, W. Cai, H. Zhang, G. Wang and H. Zhao, A nanoparticulate liquid binding phase based DGT device for aquatic arsenic measurement, *Talanta*, 2016, **160**, 225–232.

13 A. A. Menegário, L. N. M. Yabuki, K. S. Luko, P. N. Williams and D. M. Blackburn, Use of diffusive gradient in thin films for in situ measurements: a review on the progress in chemical fractionation, speciation and bioavailability of metals in waters, *Anal. Chim. Acta*, 2017, **983**, 54–66.

14 P. L. R. Van Der Veeken, J. P. Pinheiro and H. P. Van Leeuwen, Metal speciation by DGT/DET in colloidal complex systems, *Environ. Sci. Technol.*, 2008, **42**(23), 8835–8840.

15 T. Huynh, H. Zhang and B. Noller, Evaluation and Application of the Diffusive Gradients in Thin Films Technique Using a Mixed-Binding Gel Layer for Measuring Inorganic Arsenic and Metals in Mining Impacted Water and Soil, *Anal. Chem.*, 2012, **84**, 9988–9995.

16 C. Taylor, M. Matzke, A. Kroll, D. S. Read, C. Svendsen and A. Crossley, Toxic interactions of different silver forms with freshwater green algae and cyanobacteria and their effects on mechanistic endpoints and the production of extracellular polymeric substances, *Environ. Sci.: Nano*, 2016, **3**(2), 396–408.

17 A. Philippe, M. Bundschuh, S. Klitzke, D. Rakcheev, A. Grün, S. K. Kumahor, M. Kühn, W. Manz and R. Schulz, Understanding the fate and biological effects of Ag- and TiO_2-nanoparticles in the environment: the quest for advanced analytics and interdisciplinary concepts, *Sci. Total Environ.*, 2015, **535**, 3–19.

18 Bio-RAD, *Chelex 100 and Chelex 20 Chelating Ion Exchange Resin Instruction Manual*, 2012, vol. 2012.

19 *Metsorb MSDS*, Graver Technologies, 2012.

20 T. Sugimoto and X. P. Zhou, Synthesis of uniform anatase TiO_2 nanoparticles by the gel-sol method – 2. Adsorption of OH-ions to $Ti(OH)_4$ gel and TiO_2 particles, *J. Colloid Interface Sci.*, 2002, **252**, 347–353.

21 X. L. Zhu, C. W. Yuan, Y. C. Bao, J. H. Yang and Y. Z. Wu, Photocatalytic degradation of pesticide pyridaben on TiO_2 particles, *J. Mol. Catal. A: Chem.*, 2005, **229**, 95–105.

22 J. G. Panther, P. R. Teasdale, W. W. Bennett, D. T. Welsh and H. J. Zhao, Titanium Dioxide-Based DGT Technique for In Situ Measurement of Dissolved Reactive Phosphorus in Fresh and Marine Waters, *Environ. Sci. Technol.*, 2010, **44**, 9419–9424.

23 C. M. Hutchins, J. G. Panther, P. R. Teasdale, F. Wang, R. R. Stewart, W. W. Bennett and H. Zhao, Evaluation of a titanium dioxide-based DGT technique for measuring inorganic uranium species in fresh and marine waters, *Talanta*, 2012, **97**, 550–556.

24 G. S. C. Turner, G. A. Mills, P. R. Teasdale, J. L. Burnett, S. Amos and G. R. Fones, Evaluation of DGT techniques for measuring inorganic uranium species in natural waters: interferences, deployment time and speciation, *Anal. Chim. Acta*, 2012, **739**, 37–46.

25 H. M. Pouran, S. A. Banwart and M. Romero-Gonzalez, Characterizing the Cell Surface Properties of Hydrocarbon-Degrading Bacterial Strains, a Case Study, In *Handbook of Environmental Materials Management*, ed. C. Hussain, Springer, Cham, 2018, DOI: 10.1007/978-3-319-58538-3_131-2.

26 H. M. Pouran, S. A. S. A. Banwart and M. Romero-Gonzales, Coating a polystyrene well-plate surface with synthetic hematite, goethite and aluminium hydroxide for cell

mineral adhesion studies in a controlled environment, *Appl. Geochem.*, 2014, **42**(1986), 60–68.

27 J. J. Ojeda, M. E. Romero-Gonzalez, H. M. Pouran and S. A. Banwart, In situ monitoring of the biofilm formation of Pseudomonas putida on hematite using flow-cell ATR-FTIR spectroscopy to investigate the formation of inner-sphere bonds between the bacteria and the mineral, *Mineral. Mag.*, 2008, **72**(1), 101–106.

28 C. Chen, J. M. Unrine, J. D. Judy, R. W. Lewis, J. Guo, D. H. McNear and O. V. Tsyusko, Toxicogenomic Responses of the Model Legume *Medicago truncatula* to Aged Biosolids Containing a Mixture of Nanomaterials (TiO_2, Ag, and ZnO) from a Pilot Wastewater Treatment Plant, *Environ. Sci. Technol.*, 2015, **49**(14), 8759–8768.

29 G. V. Lowry, B. P. Espinasse, A. R. Badireddy, C. J. Richardson, B. C. Reinsch, L. D. Bryant, A. J. Bone, A. Deonarine, S. Chae, M. Therezien, *et al.*, Long-Term Transformation and Fate of Manufactured Ag Nanoparticles in a Simulated Large Scale Freshwater Emergent Wetland, *Environ. Sci. Technol.*, 2012, **46**(13), 7027–7036.

30 A. M. E. Badawy, T. P. Luxton, R. G. Silva, K. G. Scheckel, M. T. Suidan and T. M. Tolaymat, Impact of Environmental Conditions (pH, Ionic Strength, and Electrolyte Type) on the Surface Charge and Aggregation of Silver Nanoparticles Suspensions, *Environ. Sci. Technol.*, 2010, **44**(4), 1260–1266.

31 *AEROSIL® fumed silica*, https://products-re.evonik.com/www2/uploads/productfinder/AEROXIDE-TiO2-P-25-EN.pdf, accessed Jan 02, 2019.

32 S. Klitzke and A. Peters, The fate of silver nanoparticles in soil solution—Sorption of solutes and aggregation, *Sci. Total Environ.*, 2015, **535**, 54–60.

33 M. J. Baker, J. Trevisan, P. Bassan, R. Bhargava, H. J. Butler, K. M. Dorling, P. R. Fielden, S. W. Fogarty, N. J. Fullwood, K. A. Heys, *et al.*, Using Fourier transform IR spectroscopy to analyze biological materials, *Nat. Protoc.*, 2014, **9**(8), 1771–1791.

34 J. Trevisan, P. P. Angelov, A. D. Scott, P. L. Carmichael and F. L. Martin, IRootLab: a free and open-source MATLAB toolbox for vibrational biospectroscopy data analysis, *Bioinformatics*, 2013, **29**(8), 1095–1097.

35 F. L. Martin, J. G. Kelly, V. Llabjani, P. L. Martin-Hirsch, P. II, J. Trevisan, N. J. Fullwood and M. J. Walsh, Distinguishing cell types or populations based on the computational analysis of their infrared spectra, *Nat. Protoc.*, 2010, **5**, 1748–1760.

36 R. J. Martis, U. R. Acharya and L. C. Min, ECG beat classification using PCA, LDA, ICA and Discrete Wavelet Transform, *Biomed. Signal Process. Control*, 2013, **8**(5), 437–448.

37 R. O. Duda, P. E. Hart, E. Peter and D. G. Stork *Pattern classification*; John Wiley & Sons, 2001.

38 M. Nanosun, *13. ZnO NP Product Application Sheet*, ed. Nanosun, Micronisers, 2012.

39 W. W. Bennett, P. R. Teasdale, J. G. Panther, D. T. Welsh and D. F. Jolley, New Diffusive Gradients in a Thin Film Technique for Measuring Inorganic Arsenic and Selenium(IV) Using a Titanium Dioxide Based Adsorbent, *Anal. Chem.*, 2010, **82**, 7401–7407.

40 W. Stumm and J. J. Morgan, *Aquatic chemistry, chemical equilibria and rates in natural waters*, 1996, p. 1022.

41 H. M. Pouran, S. A. Banwart and M. Romero-Gonzales, Preparation of coated polystyrene surfaces with hematite nanoparticles to study cell-mineral adhesion under well-characterized environment, *Geochim. Cosmochim. Acta*, 2008, **72**(2), A758.

42 B. H. Stuart, Infrared Spectroscopy Fundamentals And Applications, *Methods*, 2004, **8**, 224.

43 Y. F. Gao, Y. Masuda, W. S. Seo, H. Ohta and K. Koumoto, TiO_2 nanoparticles prepared using an aqueous peroxotitanate solutions, *Ceram. Int.*, 2004, **30**, 1365–1368.

44 W. J. Kim, B. Veriansyah, J. D. Kim and S. G. Oh, Formation of titanium hydroxide nanoparticles in supercritical carbon dioxide, *J. Ceram. Process. Res.*, 2008, **9**, 88–92.